Electronic Supplementary Information (ESI)

High-performance Ni-rich $Li[Ni_{0.9-x}Co_{0.1}Al_x]O_2$ cathodes *via* multi-stage microstructural tailoring from hydroxide precursor to the lithiated oxide

Geon-Tae Park,[a] Nam-Yung Park,[a] Tae-Chong Noh,[a] Been Namkoong,[a] Hoon-Hee Ryu,[a] Ji-Yong Shin,[b] Thorsten Beierling,[c] Chong S. Yoon,*[d] and Yang-Kook Sun*[a]

[a] Department of Energy Engineering, Hanyang University, Seoul 04763, South Korea

[b] BASF Japan Ltd., 7-1-13, Doi-cho, Amagasaki 660-0083, Japan

[c] BASF SE, Carl-Bosch-Strasse 38, Ludwigshafen am Rhein 67056, Germany

[d] Department of Materials Science and Engineering, Hanyang University, Seoul 04763, South Korea

Corresponding author: csyoon@hanyang.ac.kr, yksun@hanyang.ac.kr,

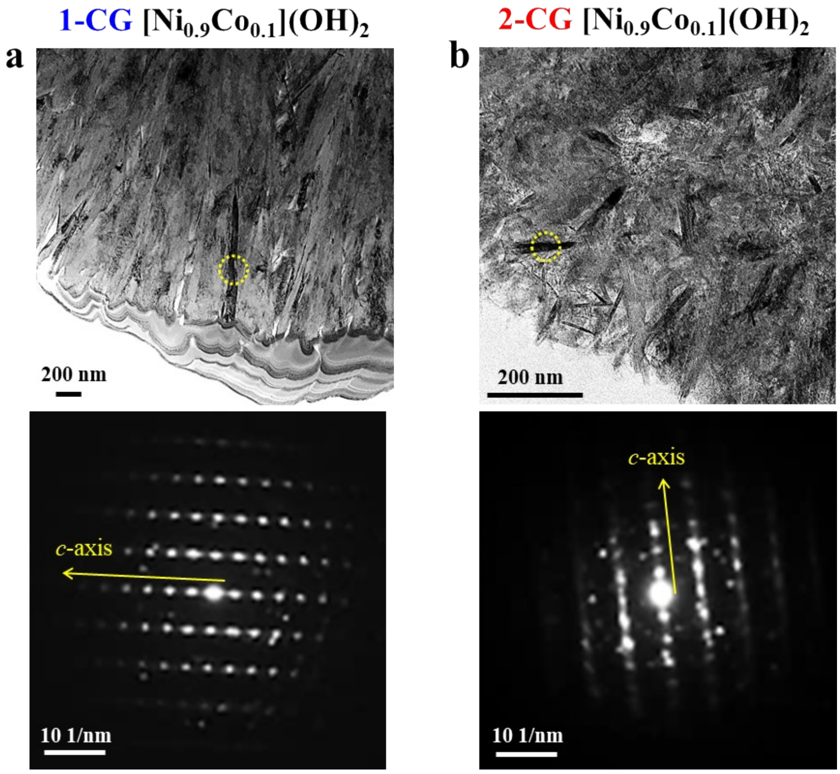

Fig. S1. Bright-field STEM images and selected area electron diffraction (SAED) patterns of marked primary particles of $[Ni_{0.9}Co_{0.1}](OH)_2$ precursors; (a) 1-CG and (b) 2-CG.

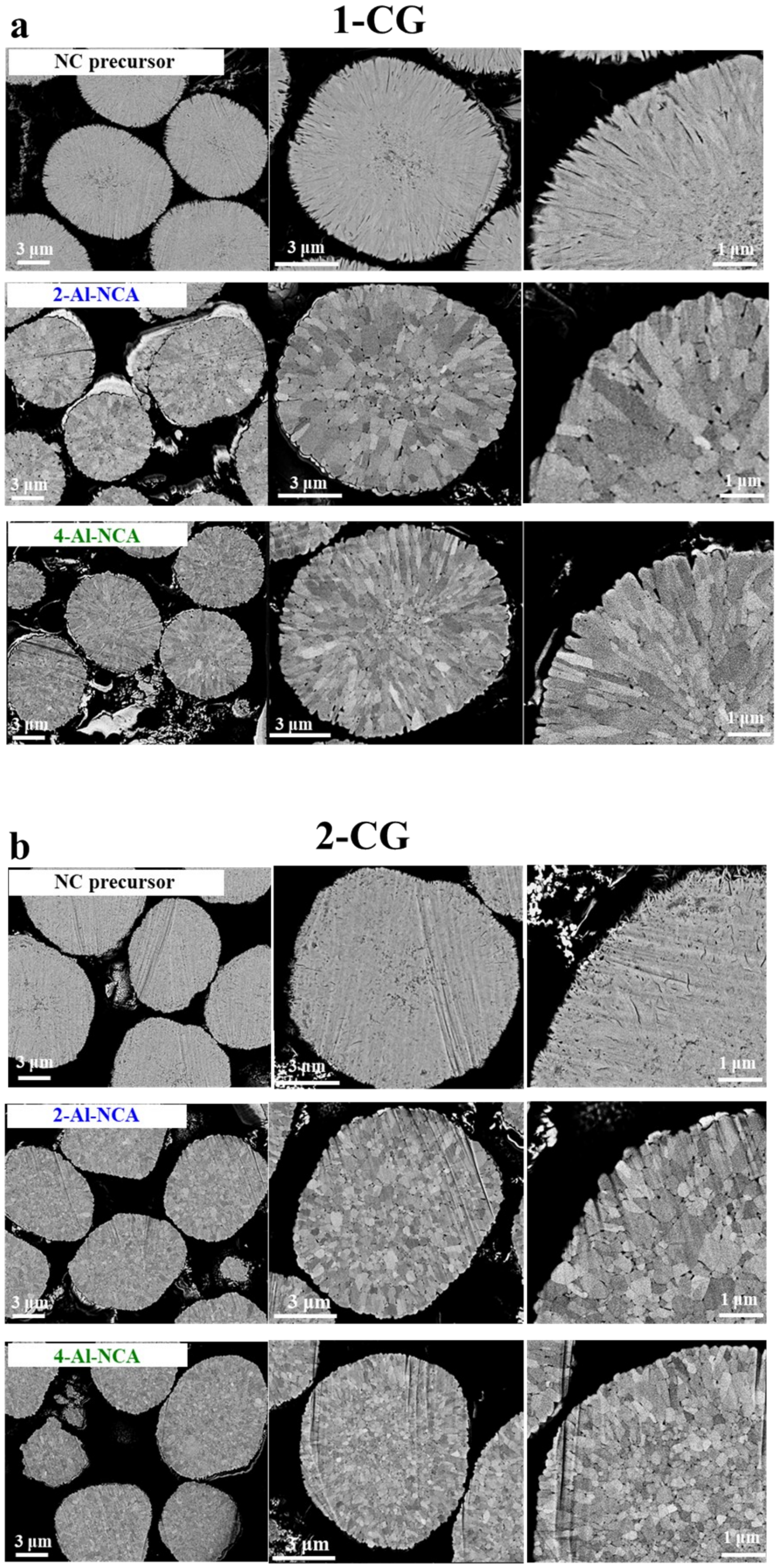

Fig. S2. Cross-sectional SEM images of $[Ni_{0.9}Co_{0.1}](OH)_2$ precursors, (a) 1-CG and (b) 2-CG, and derived 2-Al-NCA and 4-Al-NCA cathode particles.

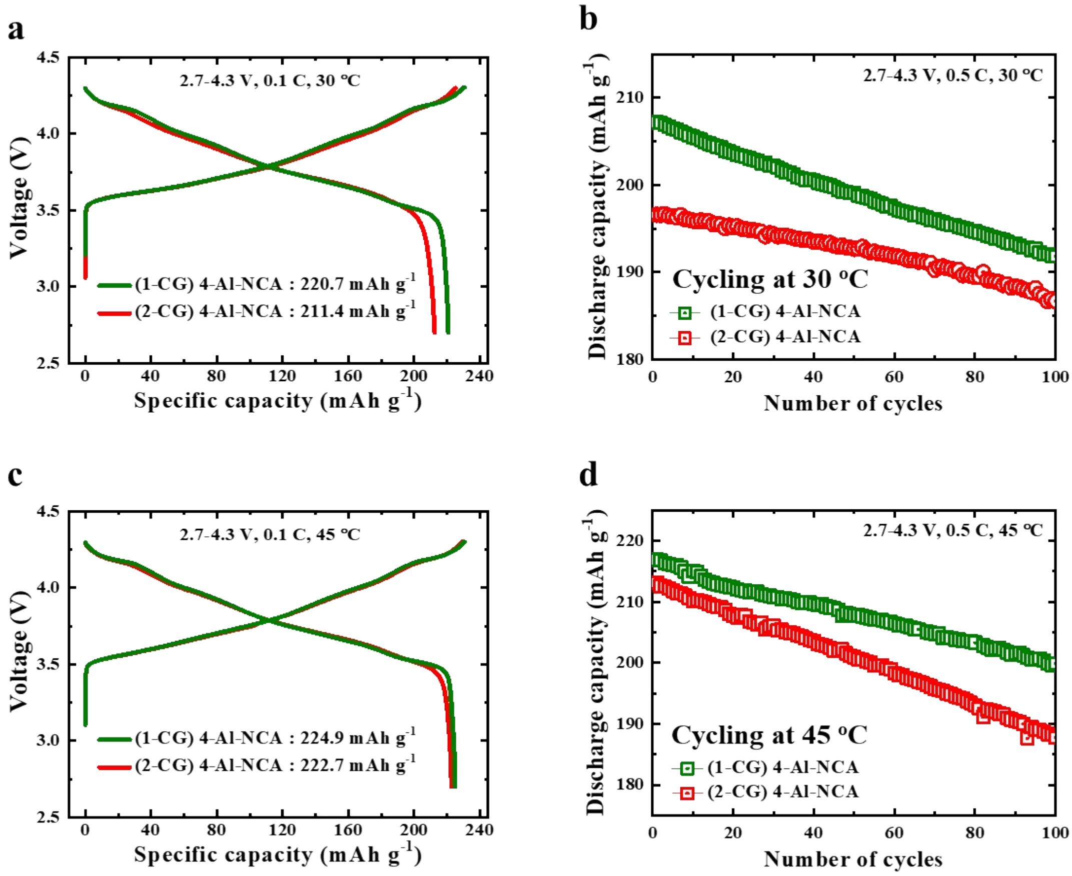

Fig. S3. Comparison of initial charge–discharge curves (at 0.1 C) at (a) 30 °C and (c) 45 °C of 4-Al-NCA cathodes derived from 1-CG and 2-CG precursors. Comparison of cycling performances (at 0.5 C) at (b) 30 °C and (d) 45 °C of 4-Al-NCA cathodes derived from 1-CG and 2-CG precursors.

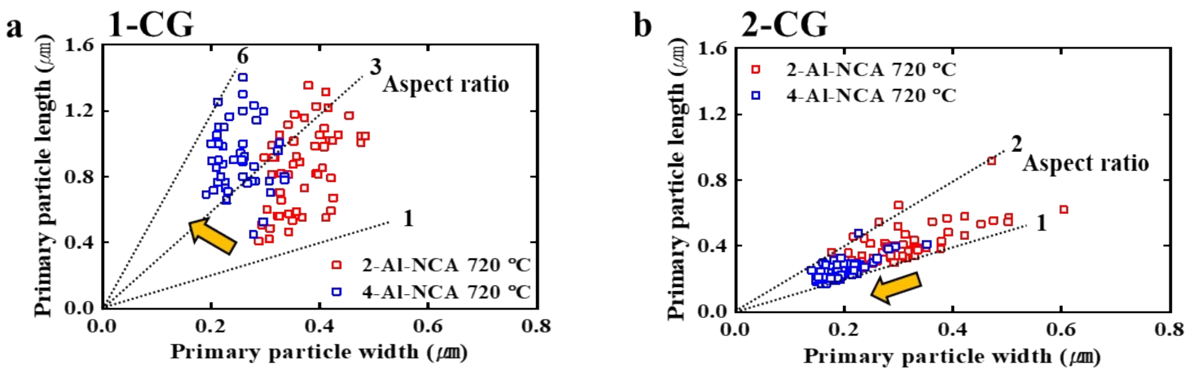

Fig. S4. Quantitative comparison of the microstructures (in terms of primary particle length, width, and aspect ratio) of 2-Al-NCA and 4-Al-NCA cathode particles derived from (a) 1-CG and (b) 2-CG precursors. The lines indicate aspect ratio of primary particle (expressed as particle length/width).

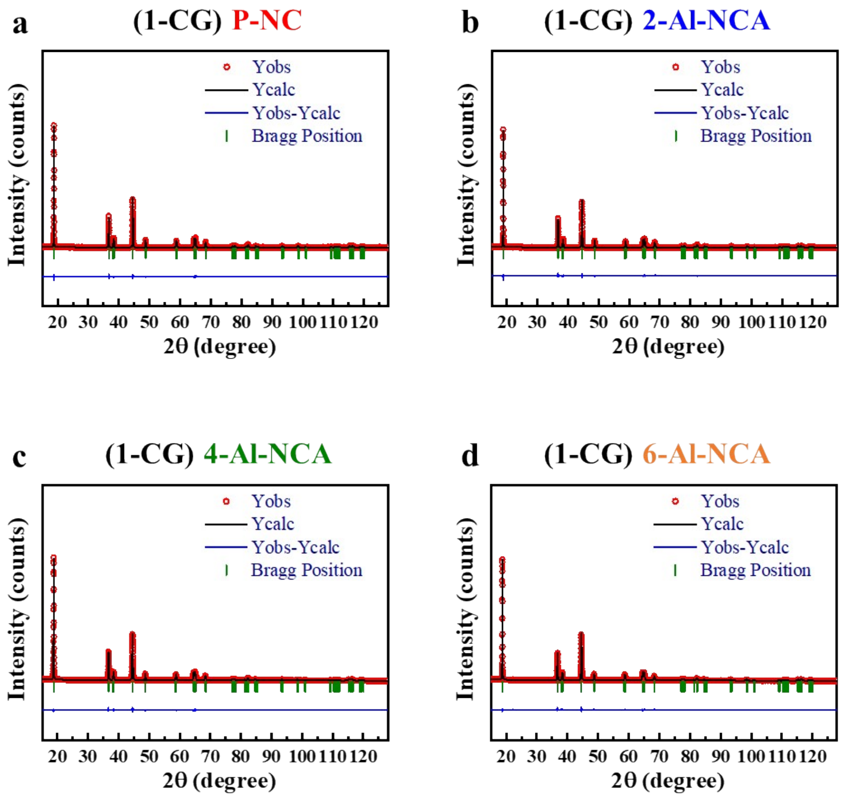

Fig. S5. Rietveld refinements of the XRD results for (a) P-NC, (b) 2-Al-NCA, (c) 4-Al-NCA, and (d) 6-Al-NCA cathodes derived from 1-CG precursors.

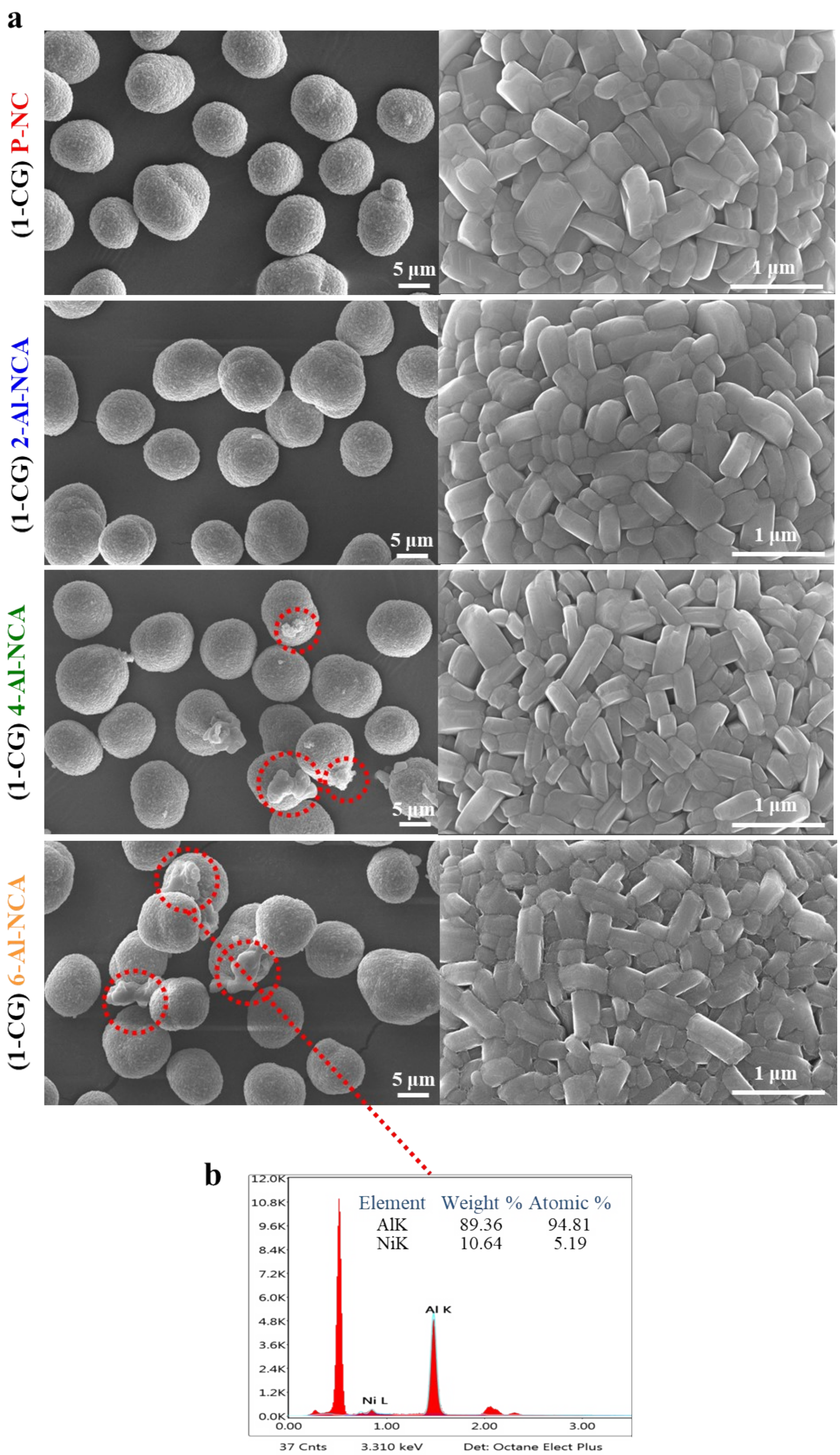

Fig. S6. (a) SEM images of P-NC, 2-Al-NCA, 4-Al-NCA, and 6-Al-NCA cathodes derived from 1-CG precursors. (b) SEM-EDS result of marked impurity particle.

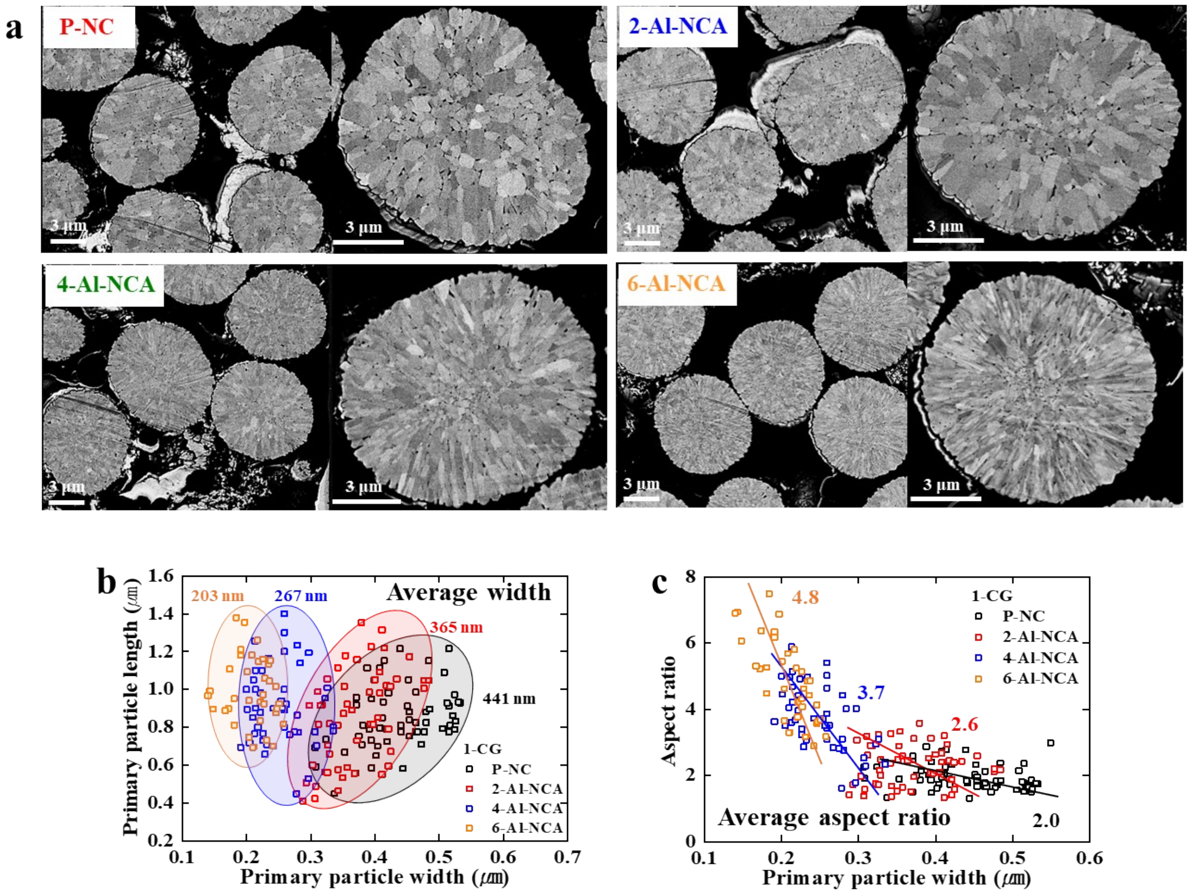

Fig. S7. (a) Cross-sectional SEM images of P-NC, 2-Al-NCA, 4-Al-NCA, and 6-Al-NCA cathodes derived from 1-CG precursors. Quantitative comparisons of the microstructures of P-NC, 2-Al-NCA, 4-Al-NCA, and 6-Al-NCA cathodes in terms of the (b) size (length and width) and (c) aspect ratio of their primary particles.

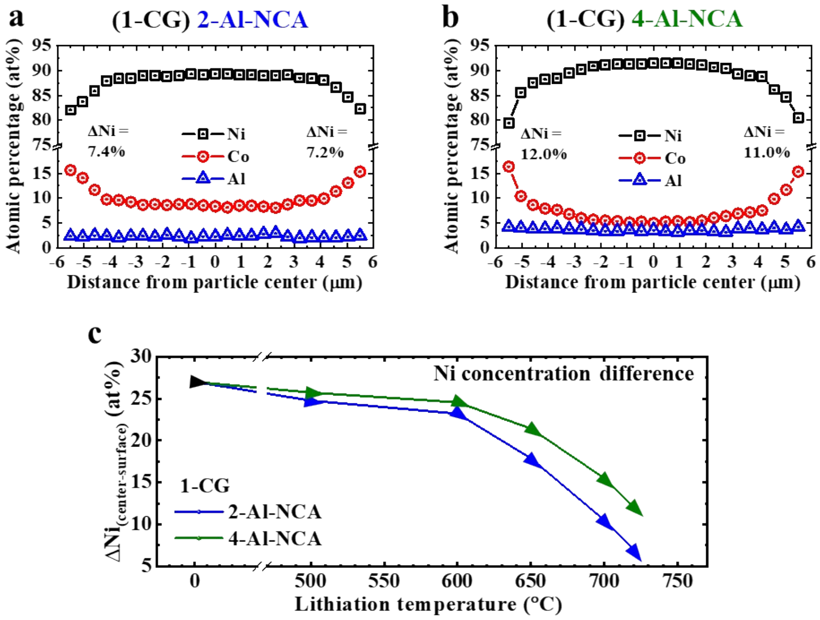

Fig. S8. Concentration gradient profiles (Ni, Co, and Al) of (a) 2-Al-NCA and (b) 4-Al-NCA cathode particles, as determined by electron probe microanalysis. (c) Comparison of Ni concentration difference between particle center and the surface of 2-Al-NCA and 4-Al-NCA cathodes as a function of lithiation temperature. The cathodes are derived from 1-CG precursors.

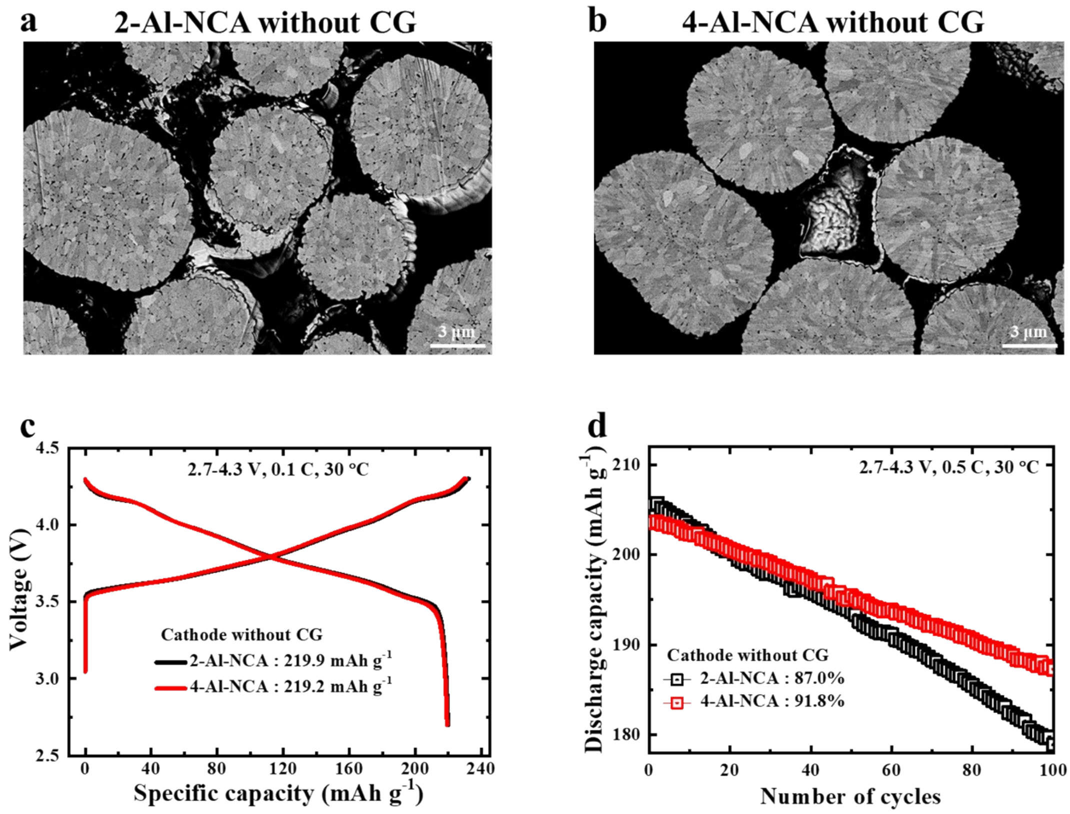

Fig. S9. Cross-sectional SEM images of (a) 2-Al-NCA, and (b) 4-Al-NCA cathode without concentration gradients. Comparison of (c) initial charge–discharge curves (at 0.1 C) and (d) cycling performance (at 0.5 C) of 2-Al-NCA and 4-Al-NCA cathodes derived from conventional precursor without concentration gradients.

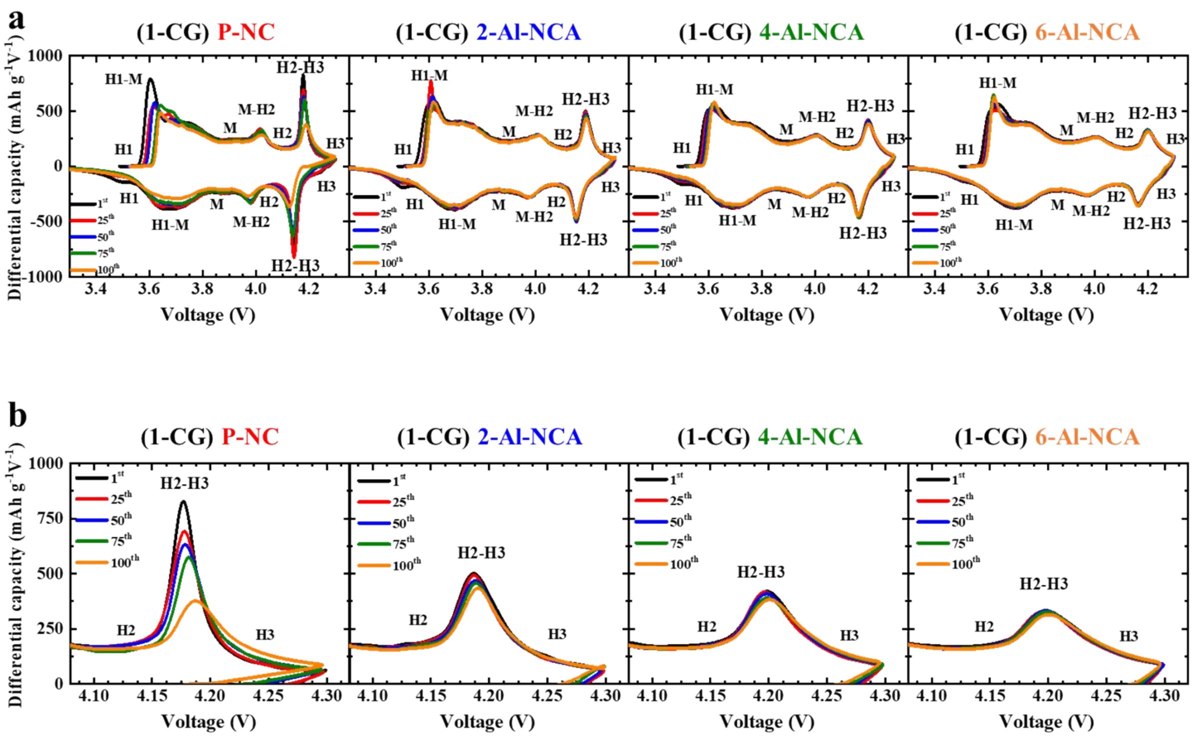

Fig. S10. (a) Differential capacity profiles of cells featuring P-NC, 2-Al-NCA, 4-Al-NCA, and 6-Al-NCA cathodes. (b) Magnified profiles during charge in the voltage range of 4.08–4.32 V. The cathodes are derived from 1-CG precursors.

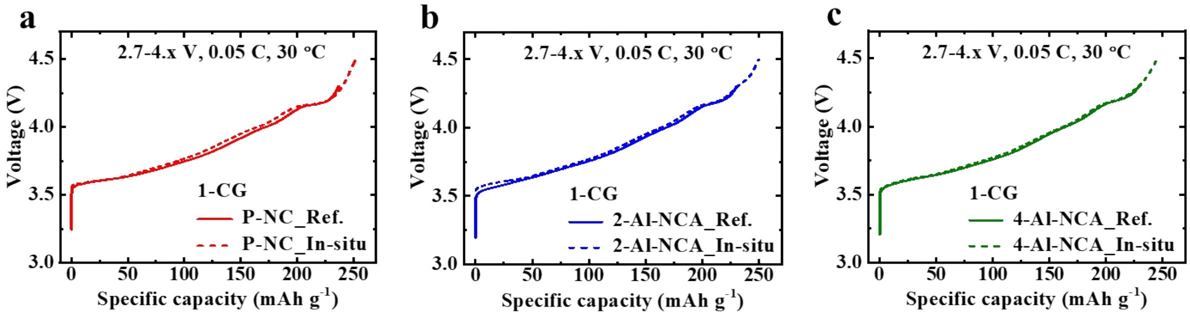

Fig. S11. Charge profiles of pouch-type half-cells (dashed lines), recorded during in situ XRD, and 2032 coin-type half-cells (solid lines) featuring (a) P-NC, (b) 2-Al-NCA, and (c) 4-Al-NCA cathodes. The cathodes are derived from 1-CG precursors.

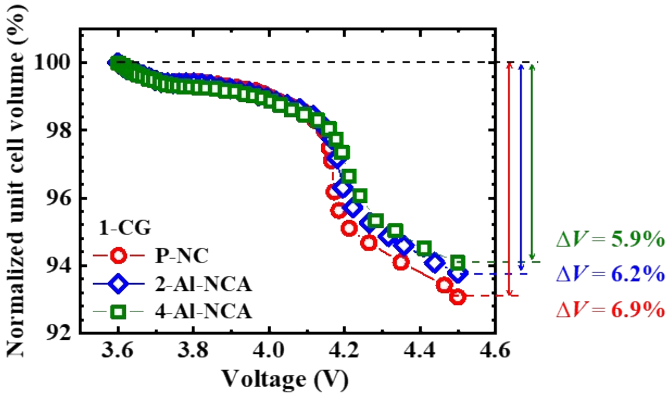

Fig. S12. Comparison of the unit cell volume changes of P-NC, 2-Al-NCA, and 4-Al-NCA cathodes during charge. The cathodes are derived from 1-CG precursors.

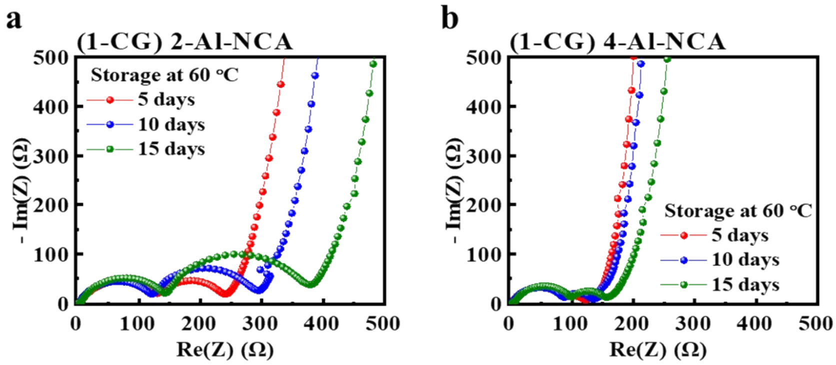

Fig. S13. Comparison of the Nyquist plots of the measured electrochemical impedances. (a) 2-Al-NCA and (b) 4-Al-NCA cathodes, charged to 4.3 V, were immersed in electrolyte (1.2 M $LiPF_6$ in EC:EMC (3:7 by vol%) with 2 wt% VC) at 60 °C for 15 days, and their electrochemical impedances were measured every 5 days. The cathodes are derived from 1-CG precursors.

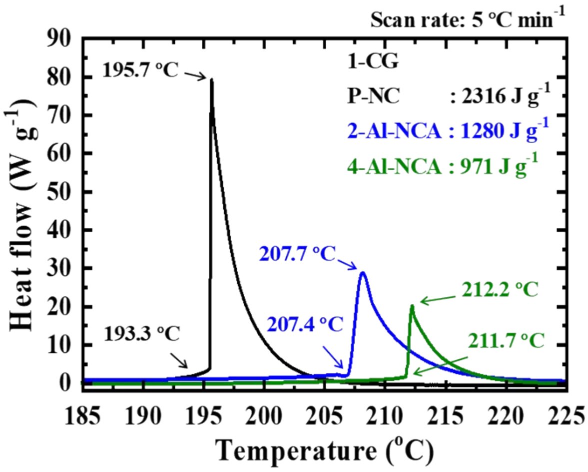

Fig. S14. Comparison of DSC thermal stability results of P-NC, 2-Al-NCA, and 4-Al-NCA cathodes charged to 4.3 V. The cathodes are derived from 1-CG precursors.

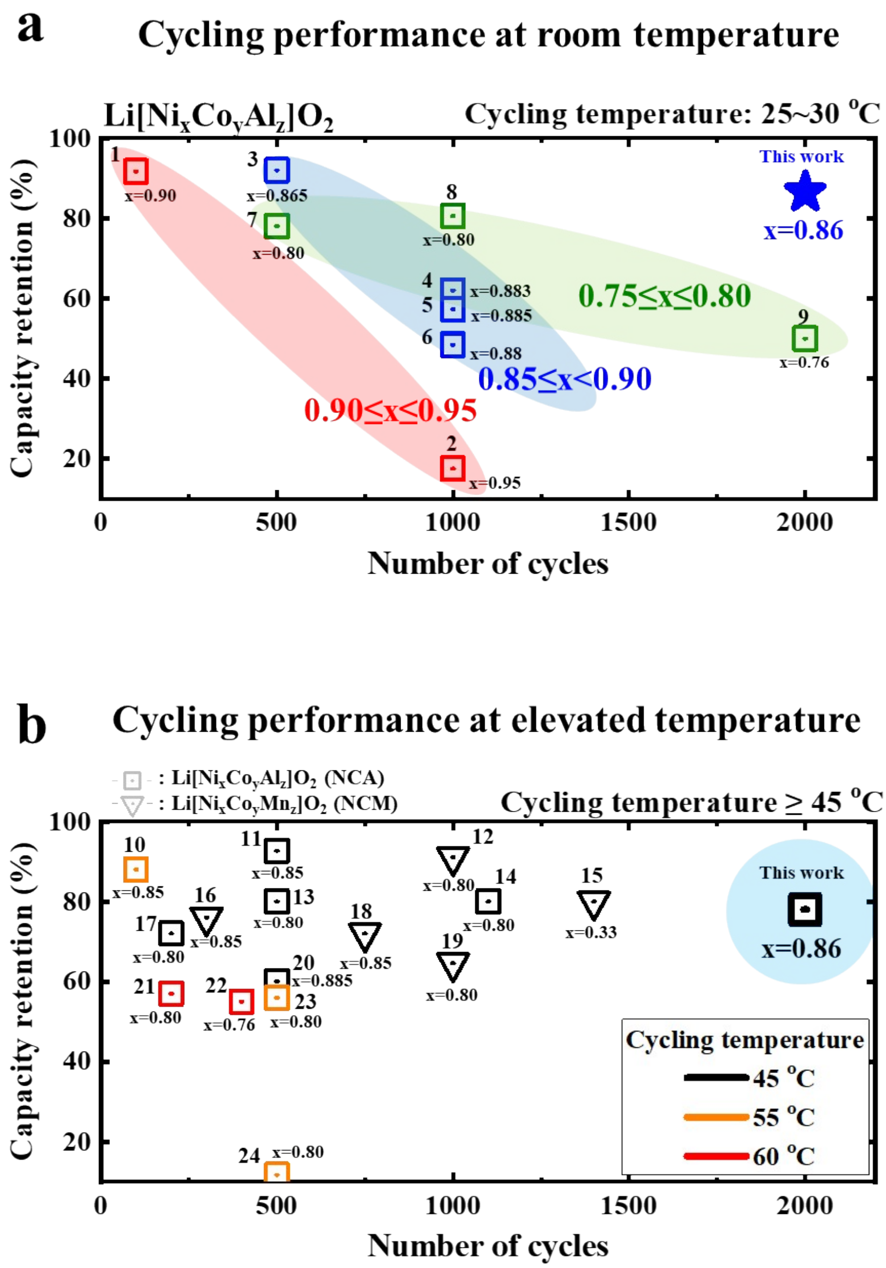

Fig. S15. The figure illustrates that the proposed Ni-rich 4-Al-NCA cathode demonstrated outstanding long-term cycling performance compared with other Ni-rich NCA and NCM cathodes reported in previous publications. Comparison of the long-term cycling performances at (a) room temperature, and (b) elevated temperature.

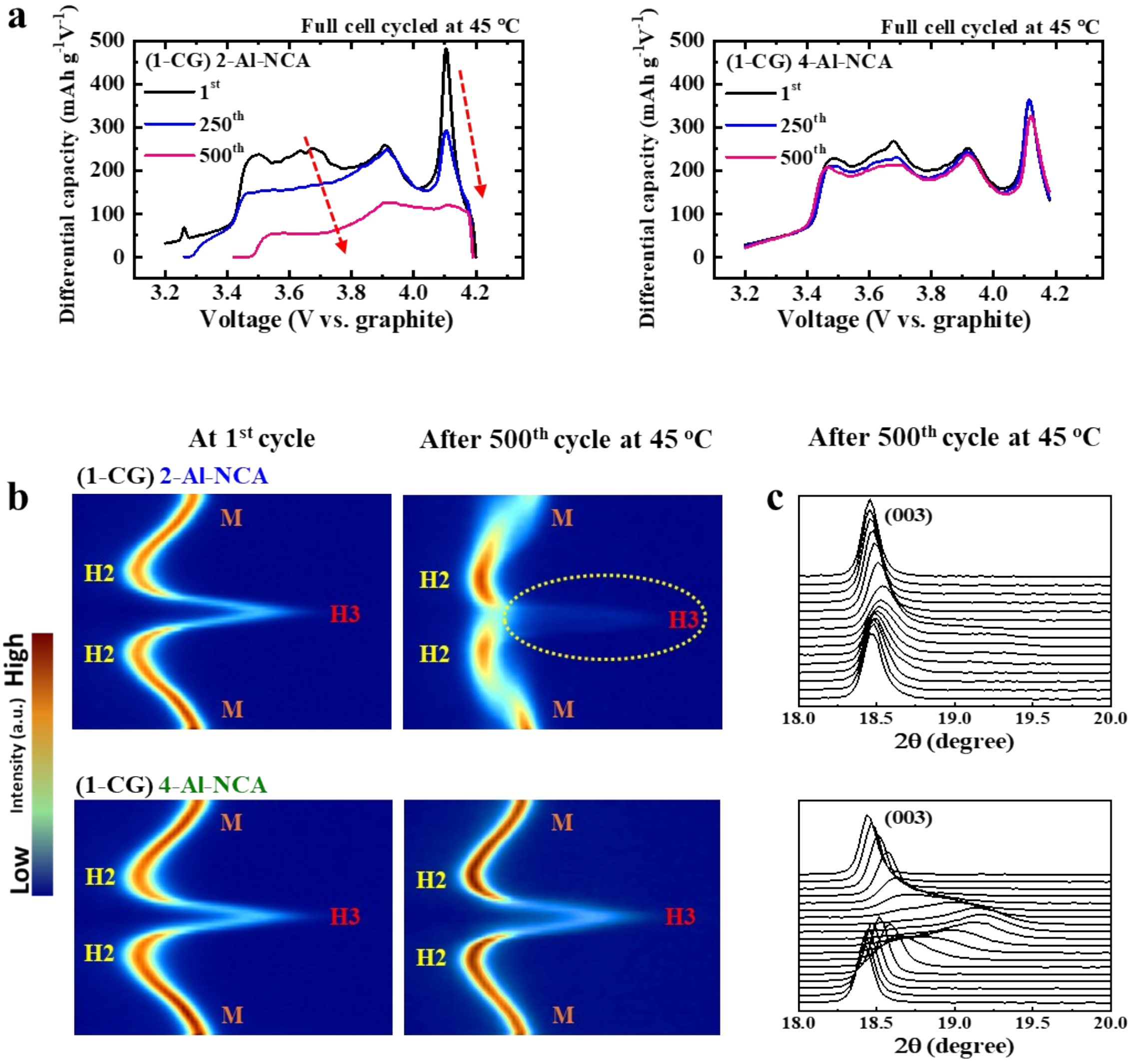

Fig. S16. (a) Differential capacity profiles of the 1st, 250th, and 500th cycles of cells featuring 2-Al-NCA and 4-Al-NCA cathodes. (b) Contour plots of (003) reflections of 2-Al-NCA and 4-Al-NCA cathodes measured during the 1st and 500th cycles at 45 °C. (c) In situ XRD patterns of 2-Al-NCA and 4-Al-NCA cathodes in the 2θ ranges of 18.0°-20.0° for the (003) reflections after 500 cycles at 45 °C. The cathodes are derived from 1-CG precursors.

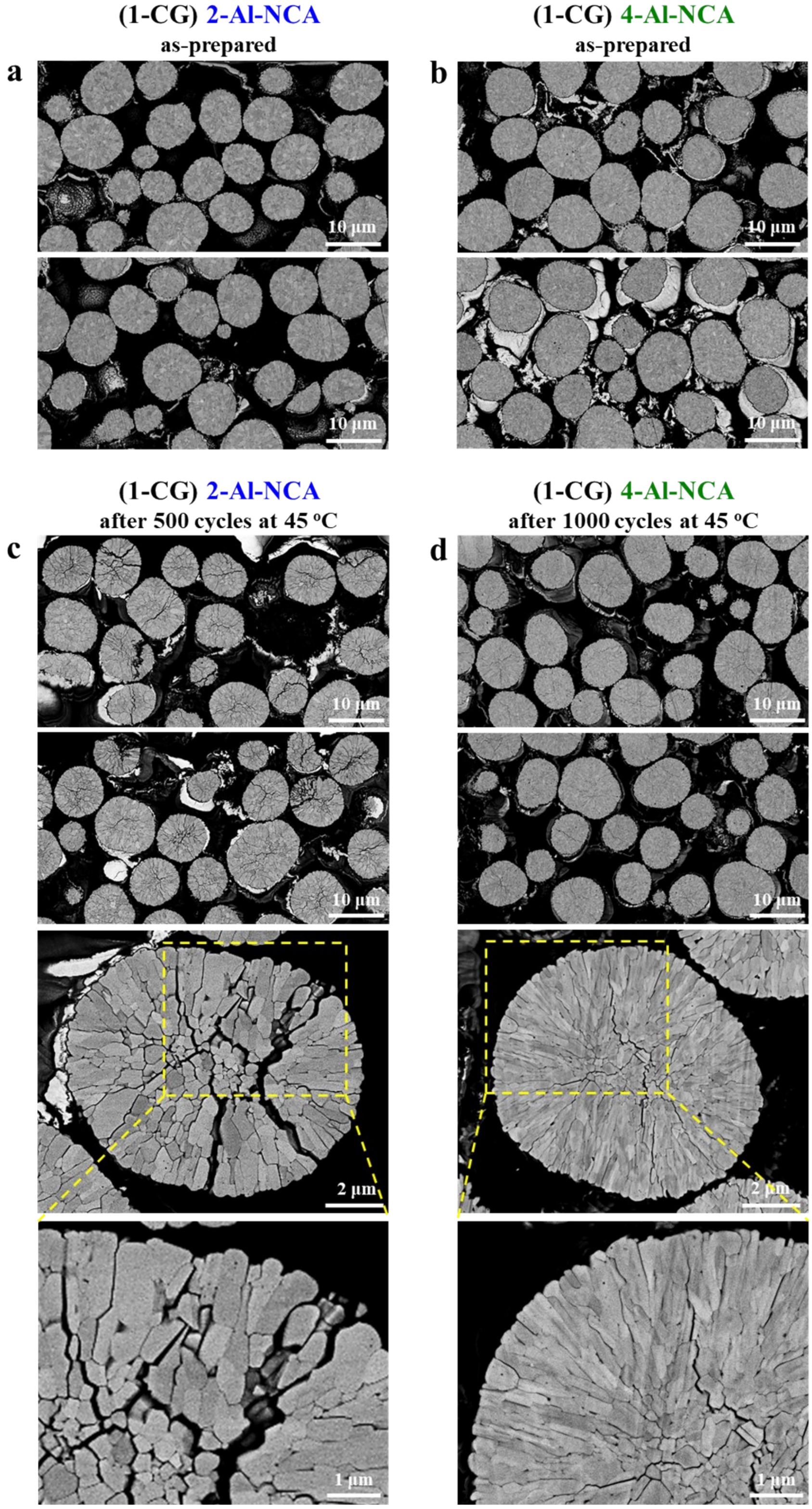

Fig. S17. Cross-sectional SEM images of as-prepared (a) 2-Al-NCA, and (b) 4-Al-NCA cathodes derived from 1-CG precursors. Comparison of the cross-sectional SEM images of (c) 2-Al-NCA cathode particles after 500 cycles and (d) 4-Al-NCA cathode particles after 1000 cycles at 45 °C. The cathodes are derived from 1-CG precursors.

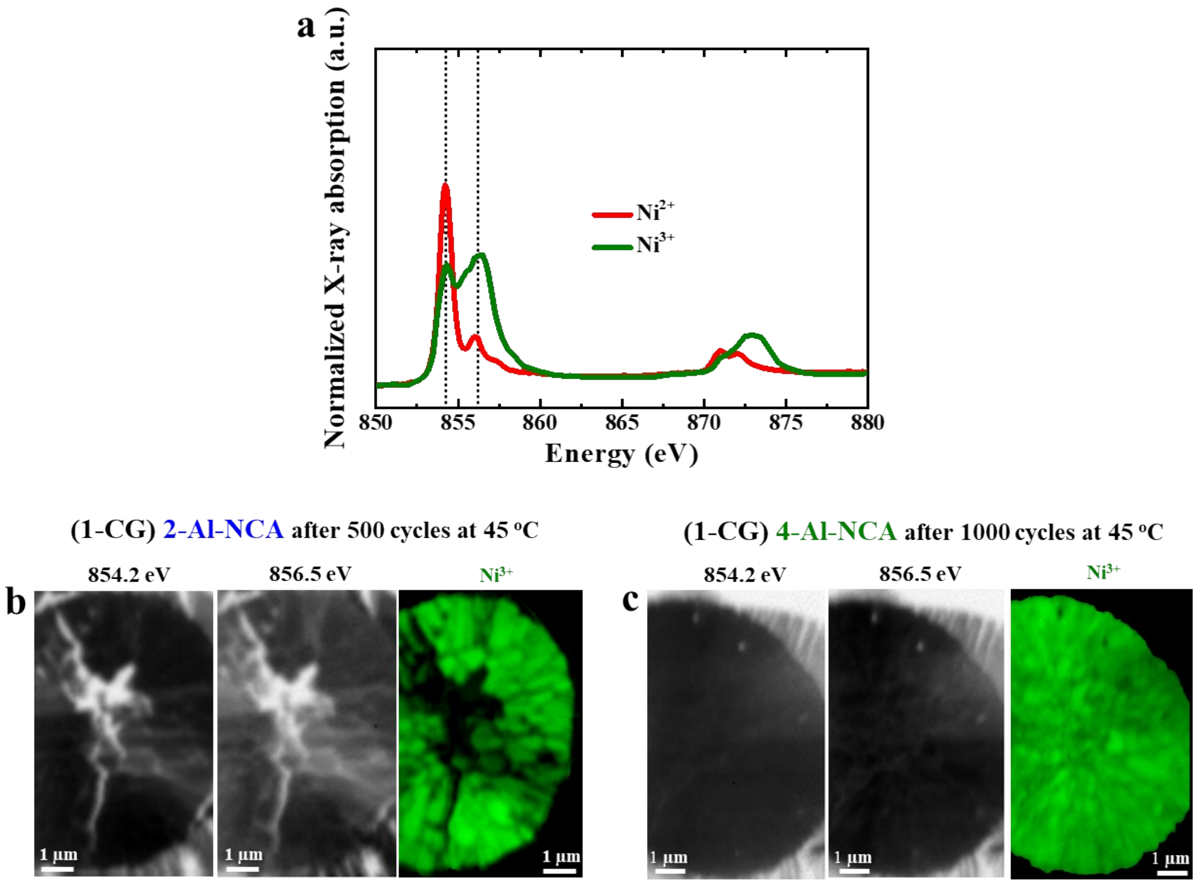

Fig. S18. (a) Reference Ni *L*-edge X-ray absorption spectra of $LiMn_{1.5}Ni_{0.5}O_4$ (Ni^{2+}, red solid line) and $LiNi_{0.8}Co_{0.15}Al_{0.05}O_2$ (Ni^{3+}, green solid line). Single-energy STXM images obtained at 854.2 and 856.5 eV, indicated by black dashed lines in (a), for the cross-sections of a fully discharged (b) 2-Al-NCA cathode particle after 500 cycles at 45 °C and (c) 4-Al-NCA cathode particle after 1000 cycles at 45 °C. The cathodes are derived from 1-CG precursors.

(1-CG) 4-Al-NCA
after 1000 cycles at 45 °C

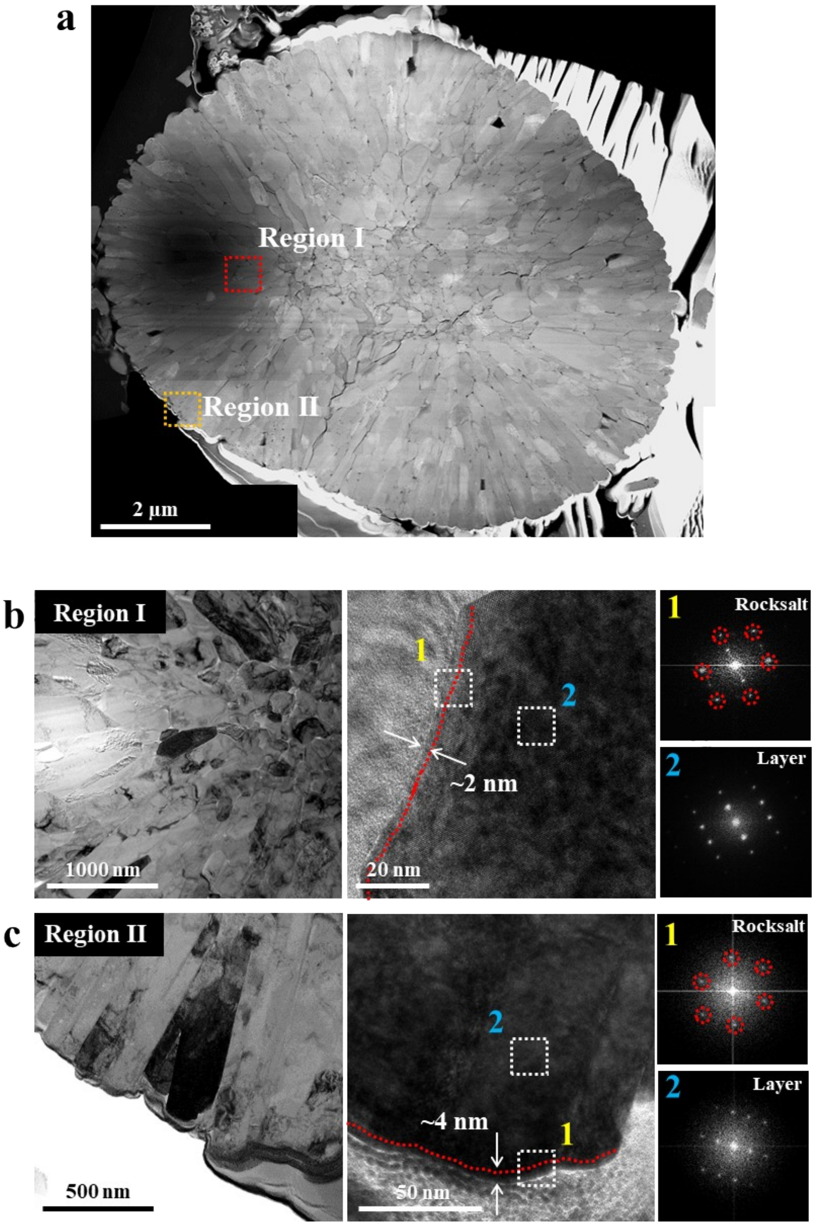

Fig. S19. Structural stability of the 4-Al-NCA cathode after 1000 cycles at 45 °C. (a) Dark-field cross-sectional STEM image of cycled 4-Al-NCA cathode. Magnified TEM images of the primary particles marked as (b) region I, (c) region II with high-resolution TEM images and corresponding fast Fourier transforms (FFTs). The cathode is derived from a 1-CG precursors.

Table S1. Chemical compositions of cathode materials determined by ICP-OES.

Precursor	Lithiation temperature	Cathode	Ni (at%)	Co (at%)	Al (at%)
1-CG	720 °C	P-NC	89.51	10.49	-
		2-Al-NCA	87.82	10.16	2.02
		4-Al-NCA	85.91	9.98	4.11
		6-Al-NCA	84.39	9.90	5.71
2-CG		2-Al-NCA	87.91	9.98	2.11
		4-Al-NCA	85.94	9.84	4.12

Table S2. Structural parameters of P-NC, 2-Al-NCA, 4-Al-NCA, and 6-Al-NCA cathodes derived from 1-CG precursors, as determined by the Rietveld refinement of the associated XRD data.

$Li[Ni_{0.90}Co_{0.10}]O_2$ (P-NC)		Space group: $R\bar{3}m$				
a-axis: 2.8688 (1) Å		c-axis: 14.1793 (2) Å		Volume: 101.061 (3) Å^3		
R_p: 2.00%	R_{wp}: 2.58%	R_{exp}: 2.04%	Chi^2: 1.61			
Atom	Wyckoff position	x	y	z	B_{iso}	*Modified occupancy
Li1	3a	0	0	0	1.000	0.992
Ni2	3a	0	0	0	1.000	0.008
Ni1	3b	0	0	0.5	0.6490	0.892
Co1	3b	0	0	0.5	0.6490	a)0.100
Li2	3b	0	0	0.5	0.6490	0.008
O1	6c	0	0	0.2420 (7)	0.7260	2

*Modified occ. = occupation *12 for Fullprof (occ.*12)

a) Fixed value

$Li[Ni_{0.88}Co_{0.10}Al_{0.02}]O_2$ (2-Al-NCA)		Space group: $R\bar{3}m$				
a-axis: 2.8668 (1) Å		c-axis: 14.1850 (1) Å		Volume: 100.961 (2) Å^3		
R_p: 1.95%	R_{wp}: 2.52%	R_{exp}: 2.04%	Chi^2: 1.52			
Atom	Wyckoff position	x	y	z	B_{iso}	*Modified occupancy
Li1	3a	0	0	0	1.000	0.992
Ni2	3a	0	0	0	1.000	0.008
Ni1	3b	0	0	0.5	0.6490	0.872
Co1	3b	0	0	0.5	0.6490	a)0.100
Al1	3b	0	0	0.5	0.6490	a)0.020
Li2	3b	0	0	0.5	0.6490	0.008
O1	6c	0	0	0.2420 (1)	0.7260	2

*Modified occ. = occupation *12 for Fullprof (occ.*12)

a) Fixed value

$Li[Ni_{0.86}Co_{0.10}Al_{0.04}]O_2$ (4-Al-NCA)	Space group: $R\bar{3}m$	

a-axis: 2.8663 (3) Å		*c*-axis: 14.1871 (1) Å		Volume: 100.941 (3) Å^3		
R_p: 1.09%	R_{wp}: 1.67%	R_{exp}: 0.77%	Chi^2: 4.66			
Atom	Wyckoff position	x	y	z	B_{iso}	*Modified occupancy
Li1	3a	0	0	0	1.000	0.993
Ni2	3a	0	0	0	1.000	0.007
Ni1	3b	0	0	0.5	0.6490	0.853
Co1	3b	0	0	0.5	0.6490	[a)]0.100
Al1	3b	0	0	0.5	0.6490	[a)]0.040
Li2	3b	0	0	0.5	0.6490	0.007
O1	6c	0	0	0.2415 (3)	0.7260	2

*Modified occ. = occupation *12 for Fullprof (occ.*12)

a) Fixed value

$Li[Ni_{0.84}Co_{0.10}Al_{0.06}]O_2$ (6-Al-NCA)		Space group: $R\bar{3}m$				
a-axis: 2.8659 (2) Å		*c*-axis: 14.1881 (1) Å		Volume: 100.920 (2) Å^3		
R_p: 1.07%	R_{wp}: 1.59%	R_{exp}: 0.78%	Chi^2: 4.12			
Atom	Wyckoff position	x	y	z	B_{iso}	*Modified occupancy
Li1	3a	0	0	0	1.000	0.991
Ni2	3a	0	0	0	1.000	0.009
Ni1	3b	0	0	0.5	0.6490	0.831
Co1	3b	0	0	0.5	0.6490	[a)]0.100
Al1	3b	0	0	0.5	0.6490	[a)]0.060
Li2	3b	0	0	0.5	0.6490	0.009
O1	6c	0	0	0.2417 (1)	0.7260	2

*Modified occ. = occupation *12 for Fullprof (occ.*12)

a) Fixed value

Table S3. Structural parameters, I(003)/I(104) XRD peak intensity ratio, and calculated crystallite size of P-NC, 2-Al-NCA, 4-Al-NCA, and 6-Al-NCA cathodes derived from 1-CG precursors.

Precursor	Cathode	*a*-axis (Å)	*c*-axis (Å)	V (Å^3)	I (003) / I (104)	*Crystallite size (nm)
1-CG	P-NC	2.8688	14.1793	101.061	2.26	113.2
	2-Al-NCA	2.8668	14.1850	100.961	2.29	104.6
	4-Al-NCA	2.8663	14.1871	100.941	2.23	79.7
	6-Al-NCA	2.8659	14.1881	100.920	2.22	78.5

* Scherrer equation (K=0.9) based on (003) reflection $\tau = \frac{K\lambda}{\beta \cos\theta}$

Table S4. Performance comparison of our 4-Al-NCA with those of other layered cathodes reported in previous publications.

Num.	Cathode material	Cathode composition	Electrolyte	Mass loading (mg/cm^2)	Voltage window (V)	Cycling temp. (^oC)	C-rate for cycling	1st discharge capacity (mAh g^{-1})	Number of cycles	Cycle retention (%)	Ref.
This work	4-Al-NCA (CG)	$Li[Ni_{0.86}Co_{0.10}Al_{0.04}]O_2$	1.2 M $LiPF_6$ in EC : EMC, 3 : 7 by vol% with 2 wt% VC	9~10	3.0-4.2	25	0.8C / 1C	182	2000	86.5	—
						45	0.8C / 1C	181.8	2000	78.0	
1	$Li[Ni_{0.9}Co_{0.07}Al_{0.03}]O_2$	$Li[Ni_{0.9}Co_{0.07}Al_{0.03}]O_2$	1.15 M $LiPF_6$ in EC : DMC : EMC, 1 : 2 : 2 by vol%	~7	2.0-4.25	25	1C	181.7	100	91.7	[1]
2	NCA95	$Li[Ni_{0.95}Co_{0.05}Al_{0.01}]O_2$	1.2 M $LiPF_6$ in EC : EMC, 3 : 7 by vol% with 2 wt% VC	~6	3.0-4.2	25	0.8C / 1C	196.7	1000	17.5	[2]
3	CSG NCA	$Li[Ni_{0.865}Co_{0.120}Al_{0.015}]O_2$	1.2 M $LiPF_6$ in EC : EMC, 3 : 7 by vol% with 2 wt% VC	—	3.0-4.2	25	0.8C / 1C	~185	500	92	[3]
4	NCA-89	$Li[Ni_{0.883}Co_{0.053}Al_{0.064}]O_2$	1.0 M $LiPF_6$ in EC : EMC, 3 : 7 by vol% with 2 wt% VC	10	2.5-4.2	25	0.5C / 1C	~185	1000	62	[4]
5	P-NCA85	$Li[Ni_{0.885}Co_{0.13}Al_{0.014}]O_2$	1.0 M $LiPF_6$ in EC : EMC, 3 : 7 by vol% with 2 wt% VC	9	3.0-4.2	25	0.8C / 1C	179.4	1000	57.3	[5]
6	NCA88	$Li[Ni_{0.88}Co_{0.10}Al_{0.02}]O_2$	1.2 M $LiPF_6$ in EC : EMC, 3 : 7 by vol% with 2 wt% VC	~6	3.0-4.2	25	0.8C / 1C	190.1	1000	48.5	[2]
7	NCA (E9)	$Li[Ni_{0.80}Co_{0.15}Al_{0.05}]O_2$	1.0 M $LiPF_6$ in EC : EMC, 3 : 7 by vol%	~8	2.5-4.3	30	0.33C / 1C	~160	500	~78	[6]
8	NCA80	$Li[Ni_{0.80}Co_{0.16}Al_{0.04}]O_2$	1.2 M $LiPF_6$ in EC : EMC, 3 : 7 by vol% with 2 wt% VC	~6	3.0-4.2	25	0.8C / 1C	173.6	1000	80.6	[2]
9	NCA	$Li[Ni_{0.76}Co_{0.14}Al_{0.10}]O_2$	1.0M $LiPF_6$ in EC,EMC,DMC	—	2.5-4.2	25	1C	—	2000	~50	[7]
10	$Li[Ni_{0.85}Co_{0.094}Al_{0.056}]O_2$	$Li[Ni_{0.85}Co_{0.094}Al_{0.056}]O_2$	1.0 M $LiPF_6$ in EC : EMC, 3 : 7 by vol% with 2 wt% VC	8	2.5-4.3	55	0.5C	~180	100	88	[8]
11	1-Nb NCA85	$Li[Ni_{0.851}Co_{0.125}Al_{0.014}Nb_{0.01}]O_2$	1.0 M $LiPF_6$ in EC : EMC, 3 : 7 by vol% with 2 wt% VC	9	3.0-4.2	45	0.8C / 1C	180.1	500	92.7	[5]
12	F1-GC80	$Li[Ni_{0.80}Co_{0.05}Mn_{0.15}]O_2$	1.2 M $LiPF_6$ in EC : EMC, 3 : 7 by vol% with 2 wt% VC	~4	3.0-4.2	45	1C	190	1000	91.1	[9]
13	$Li[Ni_{0.80}Co_{0.15}Al_{0.05}]O_2$	$Li[Ni_{0.80}Co_{0.15}Al_{0.05}]O_2$	1.0M $LiPF_6$ in EC,EMC,DMC	—	2.5-4.2	45	0.3C / 1C	—	500	~80	[10]
14	TiP2O7-coated NCA	$Li[Ni_{0.80}Co_{0.15}Al_{0.05}Ti_{0.01}]O_2$	1.0 M $LiPF_6$ in EC : EMC : DEC,3 : 3 : 4 by vol%	17.8	2.8-4.2	45	1C	—	1050	80	[11]
15	NCM	$Li[Ni_{0.33}Co_{0.33}Mn_{0.33}]O_2$	EC based electrolyte	—	3.0-4.2	45	3C	—	1400	~80%	[12]
16	$Li[Ni_{0.85}Co_{0.1}Mn_{0.05}]O_2$	$Li[Ni_{0.85}Co_{0.1}Mn_{0.05}]O_2$	1.0 M $LiPF_6$ in EC : DEC:EMC, 3 : 2 : 5 by vol% with 0.5% VC, 1% DTD, 1% LiFSI	~33	2.8-4.2	45	0.5C / 1C	—	300	76%	[13]
17	NCA (E9)	$Li[Ni_{0.80}Co_{0.15}Al_{0.05}]O_2$	1.0 M $LiPF_6$ in EC : EMC, 3 : 7 by vol%	~8	2.5-4.3	45	0.33C / 1C	~175	200	~72	[6]
18	NCM851005	$Li[Ni_{0.85}Co_{0.1}Mn_{0.05}]O_2$	1.0 M $LiPF_6$ in EC : DEC, 3 : 7 by vol% with 2 wt% VC	~10	2.8-4.2	45	1C	195	750	72%	[14]
19	GC80	$Li[Ni_{0.80}Co_{0.05}Mn_{0.15}]O_2$	1.2 M $LiPF_6$ in EC : EMC, 3 : 7 by vol% with 2 wt% VC	~4	3.0-4.2	45	1C	192	1000	64.6	[9]
20	P-NCA85	$Li[Ni_{0.885}Co_{0.13}Al_{0.014}]O_2$	1.0 M $LiPF_6$ in EC : EMC, 3 : 7 by vol% with 2 wt% VC	9	3.0-4.2	45	0.8C / 1C	180.4	500	60.1	[5]
21	NCA (E9)	$Li[Ni_{0.80}Co_{0.15}Al_{0.05}]O_2$	1.0 M $LiPF_6$ in EC : EMC, 3 : 7 by vol%	~8	2.5-4.3	60	0.33C / 1C	~180	200	~57	[6]
22	NCA	$Li[Ni_{0.76}Co_{0.14}Al_{0.10}]O_2$	$LiPF_6$ in EC,EMC,DMC	—	2.5-4.2	60	1C	—	~400	~55	[7]
23	$Li[Ni_{0.80}Co_{0.15}Al_{0.05}]O_2$	$Li[Ni_{0.80}Co_{0.15}Al_{0.05}]O_2$	1.0 M $LiPF_6$ in EC : EMC : DEC, 1 : 1 by vol%	—	3.0-4.2	55	1C	—	500	55.9	[15]
24	AlF3-coated $Li[Ni_{0.80}Co_{0.15}Al_{0.05}]O_2$	$Li[Ni_{0.80}Co_{0.15}Al_{0.05}]O_2$	1.0 M $LiPF_6$ in EC : EMC : DEC, 1 : 1 by vol%	—	3.0-4.2	55	1C	—	500	11.7	[15]

*The value was calculated based on figure given in research article.

[1] P. Zhou, H. Meng, Z. Zhang, C. Chen, Y. Lu, J. Cao, F. Cheng, and J. Chen, *J. Mater. Chem. A*, 2017, **5**, 2724.

[2] G. W. Nam, N.-Y. Park, K.-J. Park, J. Yang, J. Liu, C. S. Yoon, and Y.-K. Sun, *ACS Energy Lett.,* 2019, **4**, 2995−3001.

[3] K.-J. Park, M.-J. Choi, F. Maglia, S.-J. Kim, K.-H. Kim, C. S. Yoon, and Y.-K. Sun, *Adv. Energy Mater.*, 2018, **8**, 1703612.

[4] W. Li, S. Lee, and A. Manthiram, *Adv. Mater.*, 2020, **32**, 2002718.

[5] U.-H. Kim, J.-H. Park, A. Aishova, R. M. Ribas, R. S. Monteiro, K. J. Griffith, C. S. Yoon, and Y.-K. Sun, *Adv. Energy Mater.*, 2021, 2100884.

[6] Q. Li, S. Jiao, L. Luo, M. S. Ding, J. Zheng, S. S. Cartmell, C.-M. Wang, K. Xu, J.-G. Zhang, and, W. Xu, *ACS Appl. Mater. Interfaces*, 2017, **9**, 18826−18835.

[7] S. Watanabe, M. Kinoshita, T. Hosokawa, K. Morigaki, and K. Nakura, *J. Power Sources*, 2014, **258**, 210−217.

[8] K. Zhou, Q. Xie, B. Li, and A. Manthiram, *Energy Storage Mater.*, 2021, **34**, 229–240.

[9] U.-H Kim, G.-T Park, P. Conlin, N. Ashburn, K. Cho, Y.-S. Yu, D. A. Shapiro, F. Maglia, S.-J. Kim, P. Lamp, C.S. Yoon, and Y.-K. Sun, *Energy Environ. Sci.*, 2021, **14**, 1573–1583.

[10] S. Watanabe, M. Kinoshita, and K. Nakura, *J. Power Sources*, 2014, **247**, 412−422.

[11] G. Wu, and Y. Zhou, *J. Energy Chemistry*, 2019, **28**, 151–159.

[12] F. German, A. Hintennach, A. LaCroix, D. Thiemig, S. Oswald, F. Scheiba, M. J. Hoffmann, and H. Ehrenberg, *J. Power Sources*, 2014, **264**, 100−107.

[13] Y. Gao, D. Li, M. Yang, X. Xia, J. Long, H. Liu, L. Chen, and A. Iqbal, *Electrochim. Acta*, 2020, **359**, 136963.

[14] S. Schweidler, L. de Biasi, G. Garcia, A. Mazilkin, P. Hartmann, T. Brezesinski, and J. Janek, *ACS Appl. Energy Mater.*, 2019, **2**, 7375−7384.

[15] S.-H. Lee, C. S. Yoon, K. Amine, and Y.-K. Sun, *J. Power Sources*, 2013, **234**, 201−207.